HHS Public Access

Author manuscript

Aerosol Air Qual Res. Author manuscript; available in PMC 2017 October 12.

Published in final edited form as:

Aerosol Air Qual Res. 2017 ; 17(4): 951–964. doi:10.4209/aaqr.2016.08.0374.

Spatial Variation of Ground Level Ozone Concentrations and its Health Impacts in an Urban Area in India

Amit Kumar Gorai[1,*], **Paul B. Tchounwou**[2], and **Gargi Mitra**[1]

[1]Department of Mining Engineering, National Institute of Technology, Rourkela, Odisha-769008, India

[2]NIH/NIMHD RCMI Center for Environmental Health, College of Science, Engineering and Technology, Jackson State University, Jackson, MS 39217, USA

Abstract

The present study was designed to analyze the spatial distributions of ground-level ozone (GLO) concentrations in Ranchi (Jharkhand, India) using geostatistical approaches. From September 2014 to August 2015, monthly GLO concentrations were monitored in 40-identified locations distributed in the region of study. In every month, the monitoring was done at three different time periods of the day; 5.30 AM to 7.30 AM, 11.30 AM to 1.30 PM, and 5.30 PM to 8 PM). The time duration was assigned based on the temporal variations of GLO concentrations. The descriptive statistics indicate that the spatial mean ozone concentrations ranged from 23.45 μg m^{-3} to 53.91 μg m^{-3} in morning hours, from 82.50 μg m^{-3} to 126.66 μg m^{-3} in the day time and from 40.04 μg m^{-3} to 71.25 μg m^{-3} in the evening hours. The higher level of spatial variance observed in the months of December (standard deviation: 24.21), July (standard deviation: 29.59) and November (standard deviation: 19.60) for the morning, noon, and evening time, respectively. The effects of meteorological factors (wind speed and wind direction) on the ozone concentrations were also analysed. The study confirmed that wind speed is not the dominant factor for influencing the GLO concentrations. The study also analysed the ozone air quality index (OZAQI) for assessing the health impacts in the study area. The result suggests that most of the area had the moderate category of OZAQI (101-200) and that leads to breathing discomfort for people with lung and heart disease.

Keywords

Ground level ozone (GLO); Geostatistics; Ordinary kriging; AQI mapping; Health effect

Introduction

Air pollution is one of the challenging problems in most of the developed and developing countries (Molina and Molina, 2004; Sikder *et al.*, 2013; Al-Harbi, 2014). Consequently, it has hindered sustainable development all over the world (Han *et al.*, 2011). A marked

*Corresponding author. Tel.: +91-661-2462615 amit_gorai@yahoo.co.uk.

Supplementary Material: Supplementary data associated with this article can be found in the online version at http://www.aaqr.org.

deterioration of the air quality has been witnessed across the world due to the onset of industrialization and urbanization. It is caused by energy production from power plants, industries, residential heating, fuel burning vehicles, natural disasters, or other sources. Among all the factors, combustion of fossil fuels is one of the primary processes responsible for the continuous change in the atmospheric composition (Hassan *et al.*, 2013). The quality of air is directly or indirectly linked with all the biotic and abiotic components of the environment, and may adversely affect crops and forest ecosystems (Fuhrer, 1994; Sanders *et al.*, 1994; U.S. EPA, 1996; Schaub *et al.*, 2005; Bassin *et al.*, 2007; Hayes *et al.*, 2007; Mills *et al.*, 2007; Kampa and Castanas, 2008; Caiazzo *et al.*, 2013; Chang *et al.*, 2013).

Though a number of air pollutants (particulate matter, nitrogen dioxides, sulfur dioxide, carbon monoxide, ozone, lead, etc.) are listed as criteria pollutants in most of the country's air quality standards, the present study considers ozone for analyzing the spatial variations and its health impacts due to limitations of data availability. The presence of these pollutants in ambient air is generally due to numerous diverse and widespread sources of emissions. Ground level ozone (GLO) is considered as one of the major air pollutants due to its adverse health impacts (WHO, 2000; Han *et al.*, 2011; Hassan *et al.*, 2013). Gorai *et al.* (2014) studied the association between air pollution and asthma in New York State of the USA using GIS-based approach to estimate ozone concentrations and examined its association with asthma incidence in the study area. Poupart *et al.* (2014) conducted a study on spatio-temporal variations of ozone levels in Quebec (Canada) to compare the accuracy of three spatio-temporal models to predict summer ground-level O^3. Denby *et al.* (2010) used spatial mapping techniques to understand the trends of ozone and SO_2 in Europe. García *et al.* (2010) performed geostatistical analysis for mapping of surface-level O_3 concentration in the city of Badajoz. The study reported ozone distribution patterns in the medium size and industrialized urban city (Badajoz) in Extremadura region (southwest Spain). Carnevale *et al.* (2008) designed an integrated forecasting system using the cokriging and neural network (NNs) for forecasting maximum 8-hour ozone concentration over an urban domain in two-day advance. Awang *et al.* (2015) proposed the multivariate techniques for prediction of GLO during daytime, nighttime, and critical conversion time in urban areas. Jef *et al.* (2006) performed analysis on the spatial interpolation method for estimating the ozone concentrations over the whole territory of Belgium from sparse monitoring points distributed in the Country. Wong *et al.* (2004) compared various spatial interpolation methods for the estimation of ozone levels at census block groups using U.S. EPA's air quality monitoring data. Mulholland *et al.* (1998) studied the temporal and spatial distributions of ozone in Atlanta to establish a relation between ambient levels of ozone and pediatric asthma exacerbation. In 1997, Phillips *et al.* (1997) used interpolation techniques to determine ozone concentrations in order to estimate the exposure limit in the forests of Southeastern United States. Awang *et al.* (2016) studied the influence of spatial variability of critical conversion point (CCP) of GLO production in the context of tropical climate. The study used a hierarchical agglomerative cluster analysis (HACA) technique for analyzing the spatial variability of CCP.

The literature survey indicates that most of the studies on spatial analysis of GLO concentrations have been done in the developed countries. There are rarely any kinds of literatures available on the spatial analysis of GLO concentrations in developing countries.

Thus, the objective of the present study is to understand spatio-temporal changes of GLO concentrations in the urban area of Ranchi, Jharkhand, India. Geostatistical tools were being used to estimate the concentrations of pollutants in places where monitoring stations are not available at varied locations. The study also examined the different kriging models for obtaining spatial maps of GLO concentrations and minimizing the prediction error. In the past, many air pollution studies used deterministic method (Inverse distance weighting), but the geostatistical approach is the one that considers the spatial correlation into its estimation process (Phillips *et al.*, 1997; Buttner *et al.*, 1998). The geostatistical (kriging) method can only be used for estimating the value of a variable where a spatial correlation in the area interest exists (Hopkins *et al.* 1999; Ella *et al.*, 2001; Stein, 1999). The spatial correlation is not only a condition for interpolation of the data of ozone concentrations in space, but it also gives detailed information about the variations of the attribute (Keefer, 1994; Isaaks *et al.*, 1989; Goovaerts *et al.*, 1997; Lin *et al.*, 2009). The spatial distribution maps of ozone assist city and regional managers in identifying the areas which have harmful levels of GLO concentrations.

Materials and Method

Study Area

Ranchi municipal corporation (RMC) area (shown in Fig. 1) was selected for analyzing the spatio-temporal variations of GLO concentrations. Ranchi is the capital of the Jharkhand state. The latitude and longitude of the study area range from 85°15′9.5″E to 85°24′13″E and 23°14′ 37″N to 23°25′39.5″ N respectively. RMC consists of 55 wards covering a total area of 17,533.58 km^2. The total population in the region is approximately 843,954 (data source: Ranchi municipal corporation office, 2010). A subtropical climate exists in the study area. The climate is characterized by hot summer for three-month from March to May and rainfall during southwest monsoon from June to October. The winter months in the region are marked by dry and cold weather during the months of November to February. The altitude of the area varies from 500 to 700 m above mean sea level. The primary sources of air pollution in the city are attributed to the traffic and small scale industries.

Monitoring Instruments and Methods

For analyzing the spatial distribution, 40 sampling locations (shown in Fig. 1) distributed evenly in the study area were selected for monitoring of GLO concentrations. The instrument used for monitoring ozone concentration was Ozone Monitor (Model 202) made by 2B Tech. The latitude and longitude of each monitoring location were recorded using the GPS meter of GARMIN (Model: GPSMAP 78 series). The concentration levels had been monitored on a monthly basis at all the 40 different locations during three different periods (morning: 5.00 AM–7.30 AM, day: 11.30 AM–1.30 PM, and evening: 5.30 PM–8 PM) from September 2014 to August 2015. The specific time-period for spatial monitoring was selected based on the temporal variation of ozone concentrations. Since the monitoring had been done with a single instrument, a particular period was chosen for monitoring at 40 locations. For analyzing the temporal variation of GLO concentrations, monitoring had been conducted in a single station (Latitude: 23°20′ 56.34″ N and Longitude: 85°18′56.01″ E) (shown in Fig. 1) from 5 AM to 8 PM each month during the period of September 2014 to

August 2015. The meteorological data (temperature, wind speed and wind direction) had also been monitored using the Rainwise Automatic Weather Meter in the same period as that of ozone monitoring.

Data

Temporal Data—The diurnal variations of hourly-average GLO concentrations in each month are represented in Fig. 2. The values showed in Fig. 2 clearly indicate that the hourly average concentrations exceeded the 8-hr standard (100 μg m^{-3}) during the peak hours (11.30 AM–1.30 PM) but were within the limit of 1-hr ozone standard (180 μg m^{-3}) in each of the 12 month. The hourly variations of the GLO concentrations were compared to the hourly variations of solar radiation and ambient temperature. It was observed that the ozone concentrations were highly correlated with the temperature (r = 0.80) and solar radiation (r = 0.91). The temporal analysis helps to categorize the 24-hr period into peak hours and lean hours based on GLO concentration. The GLO concentration was found to be minimum (12.25 μg m^{-3}) in the month of November and maximum (187.5 μg m^{-3}) in the month of August. The temporal variations clearly indicate the general trend of diurnal variation, i.e., the maximum during the day hours and minimum during evening and morning hours. The daily pattern of GLO reveals that the concentration level is nearly same from 5.30 AM to 7.30 AM and attains the maximum during the post noon and again declined to the background value after the 5.30 PM. The concentration level during 11.30 AM to 1.30 PM was also shown to be at an approximately uniform values in each month. At this point, the formation and dissociation or dispersion of ozone may be in equilibrium. The peak concentrations of GLO may last for two to three hours (WHO, 1979).

Spatial Data—The present study used the geostatistical approaches for spatial analysis of GLO concentrations in the Ranchi City. Geostatistical methods use autocorrelation analysis (also called semi-variance analysis) in which the spatial auto-similarity is represented with the variogram models. In the past, many types of kriging (ordinary, simple, indicator, universal, disjunctive and probability) were developed, the present study uses the ordinary kriging for spatial analysis of GLO concentrations. Four types of semi-variogram model (spherical, exponential, Gaussian, and Stable) were examined for ordinary kriging estimations based on the 40 samples distributed in the area in each of the 12 months (September 2014–August 2015).

The descriptive statistics of the spatial data of GLO concentrations for each sampling campaign are summarized in Table 1. The results indicate that the mean values of GLO concentrations varied from 23.45 ± 15.24 μg m^{-3} to 53.91 ± 9.82 μg m^{-3} in the morning hours. Similarly, the mean values of GLO concentrations ranged from 82.50 ± 9.55 μg m^{-3} to 126.66 ± 29.59 μg m^{-3} in the day-time, and from 38.16 ± 8.59 μg m^{-3} to 161.66 ± 12.94 μg m^{-3} in the evening time. The maximum and minimum values were observed in the month of September and July respectively in the day time, and the corresponding respective months for maximum and minimum in the evening time were August and October. The higher value of standard deviation indicates the high spatial variance of GLO concentrations, and thus the mapping is very useful for assessing the health impacts. The results also suggest that the

mean values of spatial GLO concentrations did not exhibit any trend, but the concentrations were relatively lower in winter months compared to summer months.

Methods of Spatial Analysis

Exploratory Data Analysis—The first step of the kriging method is to conduct the exploratory analysis of data for checking the data consistency, outlier detection, and examining the distribution of data. The outlier detection and removal is very important for obtaining the best results from kriging interpolations. Furthermore, kriging methods give best results for the data which follows a normal distribution (Goovaerts *et al.*, 1997). If the data does not follow a normal distribution, transformations can be used to make it normal. The normality of the data was checked with the Q-Q plots (listed in supplementary file). The Q-Q plots indicate that the sampling data in each campaign closely followed a normal distribution. Thus, the study did not use the data transformation for normalization.

Structural Analysis of Data—After examining the data normality, spatial correlations were quantified with variogram (semi-variogram) models. The basic function of a semi-variogram model for a paired data values z(x) and z(x + h) with the distance lag h for continuous sampling site is given by Eq. (1) (Olea, 1999).

$$\gamma(h)=1/2E[z(x)-z(x+h)]^2 \quad (1)$$

The function for discrete sampling site is given by Eq. (2) (Olea, 1999).

$$\gamma(h)=\frac{1}{2N(h)}\sum_{i=1}^{N(h)}[z(x_i)-z(x_i+h)]^2 \quad (2)$$

where,

$z(x_i)$ represent the value of the variable z at the location of x_i,

h is the lag distance, and

N(h) represents the number of pairs of sample points separated by h.

It is very difficult to maintain the distance between the sample pairs to be exactly equal to h for irregular samples. A semivariogram plot can be obtained from the semivariogram values at different lags. The values were then fitted with the four type of semivariogram model (spherical, exponential, stable, or Gaussian). The model gives the information about the spatial structure as well as the inputs for the kriging interpolation. The variogram models and its corresponding characteristic parameters (sill, nugget, range, and lag value) for each case are listed in Table 2.

Model Prediction and Performance Evaluations—Geostatistical interpolation of ozone concentration provides the predicted value at a location where no monitoring data are available along with the prediction error, using the known concentrations. The present study uses the ordinary kriging method for prediction. The performances of the models were examined with the cross-validation results. In the cross-validation diagnostic, the ozone concentration is predicted at a particular observed location after removing the observed value at that location and using information on the remaining observations. Then the same procedure is repeated to each of the monitoring locations. Then the observed and predicted values are compared to determine the errors. The model performance evaluation was conducted using the five error indices [mean error (ME), root mean square error (RMSE), mean square error (MSE), root mean square standardized error (RMSSE), and average standard error (ASR)]. The mathematical expressions for all the five errors are represented in Eqs. (3)–(7) (Goovaerts, 1997; Gorai and Kumar, 2013). The ME should be close to zero for an unbiased prediction. The drawback of this statistics is that it depends on the scale of the data and is insensitive to inaccuracies in the variogram. Thus, the study also uses the MSE (being ideally zero) for the performance evaluation. In addition to the predictions, the kriging method also provides the kriging variances. The kriging variances used for estimating the deviations of the predicted values from the observed values. Furthermore, the closer values of RMSE and ASE indicates the good prediction. The value of RMSSE should be close to one for accurate prediction. The value of RMSSE greater than one indicates the variability of the predictions is underestimated, and for less than one, the variability is overestimated. Based on the cross-validation results, the best-fitted models were identified for each case. The maps were derived using the best-fitted model for visual presentation of the distribution of the GLO concentrations. The errors of the four different models were determined for each case and reported in Table 2. The kriging analyses were done in ArcGIS software version 10.2 with Geostatistical Analyst extension.

$$\mathrm{ME}=\frac{1}{N}\sum_{i=1}^{n}[\hat{Z}(X_i)-Z(X_i)] \quad (3)$$

$$\mathrm{MSE}=\frac{1}{N}\sum_{i=1}^{n}[\hat{Z}(X_i)-Z(X_i)]/\hat{\sigma}(X_i) \quad (4)$$

$$\mathrm{RMSE}=\sqrt{\frac{1}{n}\sum_{i=1}^{n}[\hat{Z}(X_i)-Z(X_i)]^2} \quad (5)$$

$$\mathrm{ASE}=\sqrt{\frac{1}{n}\sum_{i=1}^{n}\hat{\sigma}^2(X_i)} \quad (6)$$

$$\mathrm{RMSSE}=\sqrt{\frac{1}{n}\sum_{i=1}^{n}\left[\left\{\hat{Z}(X_i)-Z(X_i)\right\}/\hat{\sigma}^2(X_i)\right]^2} \quad (7)$$

where,

$\hat{\sigma}^2(X_i)$ is the kriging variance for location X_i,

$\hat{Z}(X_i)$ is predicted value, and

$Z(X_i)$ is the measured or observed value at location X_i (Goovaerts, 1997; ESRI, 2003).

Results and Discussion

Spatial Variations and the Effect of Meteorological Factors

The statistical analysis of spatial variations of GLO concentrations indicates that the mean spatial variations of ozone concentrations ranged from 23.45 to 53.91 μg m^{-3} during morning time, from 82.50 to 126.66 μg m^{-3} during day-time, and from 40.04 to 71.25 μg m^{-3} during evening hours.

The box plot of the spatial variation of ozone concentrations for each month is shown in Fig. 3. The box plot clearly indicates that the mean value of the spatial GLO concentration was relatively higher during daytime compared to those of the morning and evening times during each month. Also, the GLO concentration was found to be maximum in the month of July during day-time. But, there no definite trend was shown in the observed GLO concentrations with seasons. The wind rose diagrams were plotted using the hourly wind speed and wind direction data monitored during the ozone monitoring period. The wind rose diagrams for 12-month (September 2014–August 2015) are shown in Fig. 4. The plots indicate the intensity of wind speed and dominant wind direction during the sampling period. The wind rose diagram helps in the understanding of horizontal dispersion and transportation of GLO (Verma and Desai, 2008; Gorai *et al.*, 2015a, b). The plots clearly indicate that the percentage of time of calm condition of the atmosphere are low during summer and rainy seasons (May–August) in the area. Thus, the horizontal dispersion of pollutants during this period (May–August) should be higher due to more frequent wind blowing in comparison to the rest of the months. The higher dispersion of GLO leads to lower level of GLO concentration for a fixed amount of ozone formation, but in reality, the concentration level observed during these months (May–August) were not lowest. The present study did not monitor the vertical temperature profile and thus not possible to explain the vertical dispersion of pollutants. Thus, it can be inferred from the result that the wind speed does not have the dominant influence on the dispersion GLO. The local precursor sources may

dominantly influence the specific nature of spatial distribution of GLO. The present study did not monitor the vertical temperature profile and thus not possible to explain the vertical dispersion of pollutants.

Spatial Analysis

The present study examined four types (spherical, exponential, Gaussian, and stable) of variogram model for prediction of GLO concentrations at the un-sampled locations in the study area. The spatial patterns of GLO concentrations were derived using the best-fitted variogram models for each case. The best-fitted variogram models for prediction of GLO concentrations were identified based on the various prediction errors as explained in performance evaluation section. The characteristics (range, sill, and nugget value) of the best-fitted semivariogram models along with the various prediction error indices are summarized in Table 2.

The nugget effect indicates the random measurement error. However, the nugget values were found to be low in most of the cases, a significant value observed for few observed data set. The range of the variogram model varied from 2876.4 to 18538.9 m for the morning time data sets. Similarly, the variogram models ranged from 2424.4 to 18069.6 m and 2803.6 to 13170.5 m respectively for the day-time and evening-time datasets. It is also observed that the stable and exponential model yielded the best for prediction GLO concentrations in most of the cases. The spherical and Gaussian models also performed well in few cases. The percentage value of the ratio of the nugget to sill can be used for classifying the spatial dependence of the variable (Shi *et al.*, 2007; Gorai and Kumar, 2013). If the percentage ratio less than 25%, the variable (GLO) will exhibit a strong spatial dependence. The variable (GLO) indicates a moderate spatial dependence for the ratio between 25 and 75%, and weak spatial dependence for greater than 75%. In the present study, the results indicate that the GLO showed moderate to strong spatial dependence during the day-time in each month. The ratio was found to be lower than 25% in nine months and was in the range of 25–50% in three months (September, November, and June).

Similarly, the GLO showed strong spatial dependence during the morning-time in nine month and moderate spatial dependence in three months (October, January, and May). The most interesting fact that can be observed from the results is that the spatial dependence of GLO in the area is found to be weak during the evening time in many cases, i.e., the ratio was exceeded the 50% value. The number of weak, moderate, and strong spatial dependence cases during evening hours are respectively three, six, and three.

The performances of the fitted models were examined based on the calculated errors. It is clear from the results that the RMSSE values for day-time predictions were very close to 1 (desired value for perfect prediction) except in the month of September (0.82) and December (0.72). Similarly, the RMSSE values for morning-time predictions were very close to 1 except in the month of February (1.29) and April (0.77). The results further indicate that the RMSSE values for evening-time predictions were very close to 1 except in the month of July (0.77). The RMSE and ASE results indicate that the corresponding values are close to each other as desired in each case. Also, the MSE values are close to zero in each case as desired for the perfect prediction.

The spatial distribution maps were derived using the best-fitted model for each month during morning-time, day-time, and evening time. The analysis was done using Geostatistical Analyst module of ArcGIS software version 10.3. The spatial distributions of GLO concentration are presented for each month during morning-time, day-time, and evening time in Fig. (5.1)–(5.3). The maps indicate that the spatial patterns of GLO concentration in three monitoring campaign (morning, day, and evening) in a day do not have the similar trend in most of the occasions, i.e., the patterns are changes with time. This may be due to the precursor emission sources in the different zones are change with time. However, the range of the GLO concentration was found to be maximum during day-time in comparison to that of the morning and evening time. Also, the concentration range was higher during evening time in comparison to the morning time in most of the months.

The monthly spatial maps indicate that the spatial distributions of GLO concentration do not have uniform patterns in most of the cases. However, the patterns were found to be uniform in few cases due to seasonal factors. The vulnerable or the highest GLO concentrations were found in the north-east and south-west part of the study area in most of the occasions. Similarly, the safe zone or the lowest concentrations were observed in the central region of the study area in most of the occasions.

The local precursor sources may be playing the role of a specific type of distribution patterns. To identify the exact formation and dispersion of ozone, region-wise climatic conditions and precursor emissions needs to be studied.

Ozone-Air Quality Index (OZAQI) Maps for Estimation of Health Impacts

During the last two decades, a number of air quality index (AQI) determination methods have been developed worldwide (ORAQI, 1970; Ontario, 1991; GVAQI, 1997; Malaysia, 1997; UK, 1998; U.S. EPA, 1999; Sharma *et al.*, 2003; Gorai *et al.*, 2015c). Nowadays, the United States Environmental Protection Agency (US EPA) AQI system is widely recognised with few diversifications. The US EPA AQI system was designed in the year 1976 and later modified in the year of 1999.

The system uses the maximum operator function for determining the AQI values in terms of the concentrations of several representative pollutants (O_3, $PM_{2.5}$, PM_{10}, CO, SO_2, and NO_2)]. The present study uses the IND-AQI system designed by Sharma *et al.* (2003) for determining the OZAQI. The method used for determining the AQI in IND-AQI system is same as that of U.S. EPA- AQI system except the break point concentration. The breakpoints for 8-hr ozone concentration along with the ranges of various OZAQI category and the possible health consequences for Indian AQI system are summarized in Table 3. The OZAQI was determined using Eq. (8).

$$I_p = \frac{(I_{HI} - I_{LO})}{BP_{HI} - BP_{LO}}(C_P - BP_{LO}) + I_{LO} \quad (8)$$

where,

Ip represents the Index for ozone,

Cp is rounded concentration of ozone,

BP_{HI} is break point that is greater than or equal to Cp,

BP_{LO} is breakpoint that is less than or equal to Cp,

I_{HI} is OZAQI value corresponding to BP_{HI},

I_{LO} is OZAQI value corresponding to BP_{LO}.

The OZAQI values were calculated for each of monitoring locations in GIS database. Since the break points are defined only for eight-hour average concentration, it was assumed that the monitoring values in daytime represent the maximum eight-hour average values. The OZAQI maps were generated using the same interpolation method as explained above. The maps were produced only for daytime monitored values since the concentrations were lower during the morning and evening hours. The maps shown in Fig. 6 indicate that the OZAQI during the daytime are of moderate category (defined in Table 3) in most of the places during each month except in September and October. In the month of September and October, the air quality was found to be relatively better in comparison to the rest of the months. It was also reported that moderate category of OZAQI (defined in Table 3) leads to breathing discomfort for people with lung and heart disease.

Conclusions

The present study analyzed the temporal and spatial variations of GLO concentrations in Ranchi City, India. The temporal variations data revealed that GLO concentration slowly rises after the sun rise and attains the maximum during the post noon time and again declines to the background level after the sun set. The peak levels of ozone concentrations in each month were within the limit of 1-hr National Ambient Air Quality Standard (NAAQS), India. The mean value of the spatial GLO concentration was found to be relatively higher during daytime in comparison to that of the morning and evening hours in each month. There was no definite trend exists in the observed GLO with months. The wind-rose diagrams indicate that the percentage of time of calm condition of the atmosphere is low during summer and rainy seasons (May–August) in the region. Thus, the horizontal dispersion of pollutants during this period should be higher during summer and rainy seasons in comparison to the rest of the months. The higher dispersion of GLO leads to lower level of GLO concentration for a fixed amount of ozone formation, but in reality, the concentration level observed during these months were not lowest. Thus, it can be inferred from the result that the wind speed does not have the dominant influence on the dispersion GLO.

The maps indicate that the spatial patterns of GLO concentration in three monitoring campaign (morning, day, and evening) in a day do not have similar trend in most of the occasions, i.e., the patterns are changes with time. This may be due to the precursor emission sources in different area are changes with time.

The monthly spatial maps indicate that the spatial distributions of GLO concentration do not have uniform patterns in most of the cases. However, the patterns were found to be uniform in few cases due to seasonal factors. The vulnerable zone or area of highest concentrations was generally found in the north-east and south-west parts of the study area. Conversely, the central region had the lowest concentrations and was considered to be the safe zone. The results of OZAQI maps indicate that OZAQI during the daytime are of moderate category in most of the places in each month except in September and October. The moderate category of OZAQI leads to breathing discomfort for people with lung and heart disease.

The major limitation of the study is related to the non-availability of station-wise meteorological data and vertical temperature profile. These data may help in detailed dispersion analysis of the GLO.

Supplementary Material

Refer to Web version on PubMed Central for supplementary material.

Acknowledgments

The authors would like to acknowledge the financial support (Grant No. SR/FTP/ES-17/2012) from the Department of Science and Technology, New Delhi. The support of NIH/NIMHD Grant No. G12MD007581 is also acknowledged.

References

Al-Harbi M. Assessment of air quality in two different urban localities. Int J Environ Res Public Health. 2014; 8:15–26.

Awang NR, Elbayoumi M, Ramli NA, Yahaya AS. The influence of spatial variability of critical conversion point (CCP) in production of ground level ozone in the context of tropical climate. Aerosol Air Qual Res. 2016; 16:153–165.

Awang NR, Ramli NA, Yahaya AS, Elbayoumi M. Multivariate methods to predict ground level ozone during daytime, nighttime, and critical conversion time in urban areas. Atmos Pollut Res. 2015; 6:726–734.

Bassin S, Volk M, Fuhrer J. Factors affecting the ozone sensitivity of temperate European grasslands: An overview. Environ Pollut. 2007; 146:678–691. [PubMed: 16904248]

Büttner O, Becker A, Kellner S, Kuehn B, Wendt-Potthoff K, Zachmann DW, Friese K. Geostatistical analysis of surface sediments in an acidic mining lake. Water Air Soil Pollut. 1998; 108:297–316.

Caiazzo F, Ashok A, Waitz IA, Yim SH, Barrett SR. Air pollution and early deaths in the United States. Part I: Quantifying the impact of major sectors in 2005. Atmos Environ. 2013; 79:198–208.

Carnevale, C., Finzi, G., Pisoni, E., Singh, V., Volta, M. Neural networks and co-kriging techniques to forecast ozone concentrations in urban areas. Proc. iEMSs 4th Biennial Meeting - International Congress on Environmental Modelling and Software, Integrating Sciences and Information Technology for Environmental Assessment and Decision Making, iEMSs 2008; Bercelona, Spain. 2008. p. 1125-1132.

Chang CJ, Yang HH, Chang CA, Tsai HY. Volatile organic compounds and nonspecific conjunctivitis: A population-based study. Aerosol Air Qual Res. 2013; 13:237–242.

Denby B, Sundvor I, Cassiani M, de Smet P, de Leeuw F, Horálek J. Spatial mapping of ozone and SO_2 trends in Europe. Sci Total Environ. 2010; 408:4795–4806. [PubMed: 20619880]

Ella VB, Melvin SW, Kanwar RS. Spatial analysis of NO_3-N concentration in glacial till. Trans ASAE. 2001; 44:317–327.

ESRI. [Last Access: December 2015] ArcGIS 9. Using ArcGIS Geostatistical Analyst. 2003. http://forums.esri.com/Thread.asp?c=93&f=1727&t=257926

Fuhrer, J. Critical levels for ozone: A UNECE workshop report, Schriftreihe der Les Cahiers de la FAC Liebefeld 16. Liebefeld-Bern, Switzerland: 1994. The critical level for ozone to protect agricultural crops: An assessment of data from European open-top chamber experiments; p. 42-57.

García F, González VV, Rodríguez FL. Geostatistical analysis and mapping of ground-level ozone in a medium sized urban area. Int J Civil Environ Eng. 2010; 2:71–82.

Goovaerts, P. Geostatistics for Natural Resources Evaluation. Oxford University Press; 1997. Applied Geostatistics Series

Gorai AK, Kumar S. Spatial distribution analysis of groundwater quality index using GIS: A case study of Ranchi municipal corporation (RMC) area. Geoinfor Geostat An Overview. 2013; 1:2.

Gorai AK, Tuluri F, Tchounwou PB. A GIS based approach for assessing the association between air pollution and asthma in New York State, USA. Int J Environ Res Public Health. 2014; 11:4845–4869. [PubMed: 24806193]

Gorai AK, Tuluri F, Tchounwou PB. Development of PLS–path model for understanding the role of precursors on ground level ozone concentration in Gulfport, Mississippi, USA. Atmos Pollut Res. 2015a; 6:389–397.

Gorai AK, Tuluri F, Tchounwou PB, Ambinakudige S. Influence of local meteorology and NO_2 conditions on ground level ozone concentration in eastern part of Texas, USA. Air Qual Atmos Health. 2015b; 8:81–96. [PubMed: 25755687]

Gorai AK, Tuluri F, Upadhyay A, Kanchan Goyal P, Tchounwou PB. An innovative approach for determination of air quality health index. Sci Total Environ. 2015c; 533:495–505. [PubMed: 26186464]

GVAQI. Greater Vancouver Regional District Air Quality and Source Control Department. Burnaby, BC, Canada: 1997.

Han S, Bian H, Feng Y, Liu A, Li X, Zeng F, Zhang X. Analysis of the Relationship between O_3, NO and NO_2 in Tianjin, China. Aerosol Air Qual Res. 2011; 11:128–139.

Hassan IA, Basahi JM, Ismail IM, Habeebullah TM. Spatial distribution and temporal variation in ambient ozone and its associated NO_x in the atmosphere of Jeddah City, Saudi Arabia. Aerosol Air Qual Res. 2013; 13:1712–1722.

Hayes, F., Mills, G., Harmens, H., Norris, D. Evidence of Widespread Ozone Damage to Vegetation in Europe (1990-2006). ICP Vegetation Programme Coordination Centre; CEH Bangor, UK: 2007.

Hopkins LP, Ensor KB, Rifai HS. Empirical evaluation of ambient ozone interpolation procedures to support exposure models. J Air Waste Manage Assoc. 1999; 49:839–846.

Isaaks, EH., Srivastava, RH. An Introduction to Applied Geostatistics. Oxford University Press; New York: 1989.

Jef H, Clemens M, Gerwin D, Frans F. Spatial interpolation of ambient ozone concentrations from sparse monitoring points in Belgium. J Environ Monit. 2006; 8:1129–1135. [PubMed: 17075619]

Kampa M, Castanas E. Human health effects of air pollution. Environ Pollut. 2008; 151:362–367. [PubMed: 17646040]

Keefer DK. The importance of earthquake-induced landslides to long term slope erosion and slope-failure hazards in seismically active regions. Geomorphology. 1994; 10:265–284.

Lin YP, Chu HJ, Wang CL, Yu HH, Wang YC. Remote sensing data with the conditional Latin hypercube sampling and geostatistical approach to delineate landscape changes induced by large chronological physical disturbances. Sensors. 2009; 9:148–174. [PubMed: 22389593]

Malaysia. A Guide to Air Pollutant Index in Malaysia. Department of Environment, Ministry of Science, Technology and the Environment; Kuala Lumpur, Malaysia: 2000. https://aqicn.org/images/aqi-scales/malaysia-api-guide.pdf [Last Access: July, 2014]

Mills G, Buse A, Gimeno B, Bermejo V, Holland M, Emberson L, Pleijel H. A synthesis of AOT40-based response functions and critical levels of ozone for agricultural and horticultural crops. Atmos Environ. 2007; 41:2630–2643.

Molina MJ, Molina LT. Megacities and atmospheric pollution. J Air Waste Manage Assoc. 2004; 54:644–680.

Mulholland JA, Butler AJ, Wilkinson JG, Russell AG, Tolbert PE. Temporal and spatial distributions of ozone in Atlanta: Regulatory and epidemiologic implications. J Air Waste Manage Assoc. 1998; 48:418–426.

Olea, RA. Geostatistics for Engineers and Earth Scientists. Kluwer Academic Publishers; Boston: 1999.

Ontario. A Guideline to the Ontario Air Quality Index System. Ontario Ministry of the Environment; Toronto: 1991. Ont. Canada0-7729-8230-9 Air Resource Branch. https://archive.org/stream/guidetoontarioai00mignuoft/guidetoontarioai00mignuoft_djvu.txt [Last Access: July, 2014]

ORAQI. Oak Ridge Air Quality Index. In: Ott, WR., editor. Environmental Indices Theory and Practice. Ann Arbor Science; Mich: 1970.

Phillips DL, Lee EH, Herstrom AA, Hogsett WE, Tingey DT. Use of Auxiliary data for spatial interpolation of ozone exposure in Southeastern Forests. Environmetrics. 1997; 8:43–61.

Poupart AA, Brand A, Fournier M, Jerrett M, Smargiass A. Spatiotemporal modeling of ozone levels in Quebec (Canada): A comparison of kriging, land-use regression (LUR), and combined Bayesian maximum entropy-LUR approaches. Environ Health Perspect. 2014; 122:970–976. [PubMed: 24879650]

Ranchi Municipal Corporation (RMC). Ward-wise population data of 2010 in RMC obtained through personal request at the office.

Sanders, G., Balls, G., Booth, C. Ozone critical levels for agricultural crops: Analyses and interpretation of the results from the UNECE international co-operative programme for crops, critical levels for ozone: A UNECE workshop report, Schriftreihe der Les Cahiers de la FAC Liebefeld 16. Liebefeld-Bern, Switzerland: 1994. p. 58-72.

Schaub M, Skelly JM, Zhang JW, Ferdinand JA, Savage JE, Stevenson RE, Davis DD, Steiner KC. Physiological and foliar symptom response in the crowns of Prunus serotina, Fraxinus americana and Acer rubrum canopy trees to ambient ozone under forest conditions. Environ Pollut. 2005; 133:553–567. [PubMed: 15519730]

Sharma M, Maheshwari M, Sengupta B, Shukla BP. Design of a website for dissemination of air quality index in India. Environ Modell Software. 2003; 18:405–411.

Shi J, Wang H, Xu J, Wu J, Liu X, Zhu H, Yu C. Spatial distribution of heavy metals in soils: A case study of Changxing, China. Environ Geol. 2007; 52:1–10.

Sikder HA, Nasiruddin M, Suthawaree J, Kato S, Kajii Y. Long term observation of surface O_3 and its precursors in Dhaka, Bangladesh. Atmos Res. 2013; 122:378–390.

Stein, ML. Interpolation of Spatial Data: Some Theory for Kriging. Springer; 1999. Series in Statistics

U.S Environmental Protection Agency. Review of national ambient air quality standards for ozone: Assessment of scientific and technical information, Office of Air Quality Planning and Standards, Report No EPA-452/R-R-07-007. Research Triangle Park; NC: 1996.

U.S Environmental Protection Agency. Office of Air Quality Planning and Standards. Research Triangle Park; NC 27711: 1999. Guideline for reporting of daily air quality - air quality index (AQI). EPA-454/R-99-010.

UK. Air Pollution - what it means for your health. Department of the Environment, Transport and the Regions; PO BOX No 236, Wetherby LS23 7NB, U.K: 1998.

Verma SS, Desai B. Effect of meteorological conditions on air pollution of Surat city. J Int Environ Appl Sci. 2008; 3:358–367.

WHO. Guidelines for Air Quality. World Health Organization; Geneva: 2000. p. 190

Wong DW, Yuan L, Perlin SA. Comparison of spatial interpolation methods for the estimation of air quality data. J Exposure Sci Environ Epidemiol. 2004; 14:404–415.

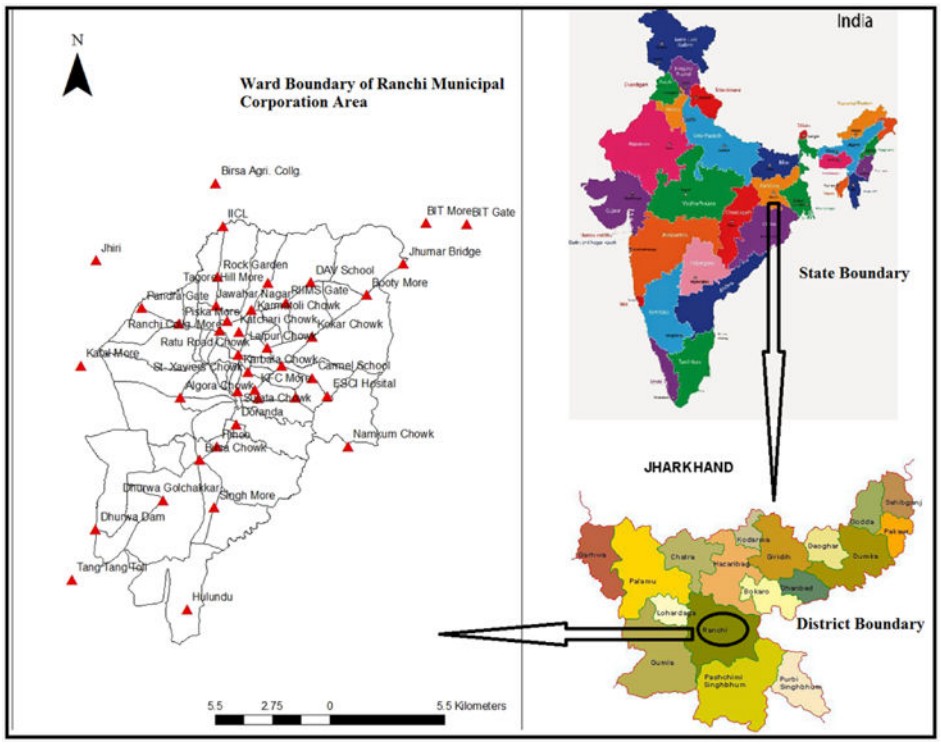

Fig. 1.
Study Area Map.

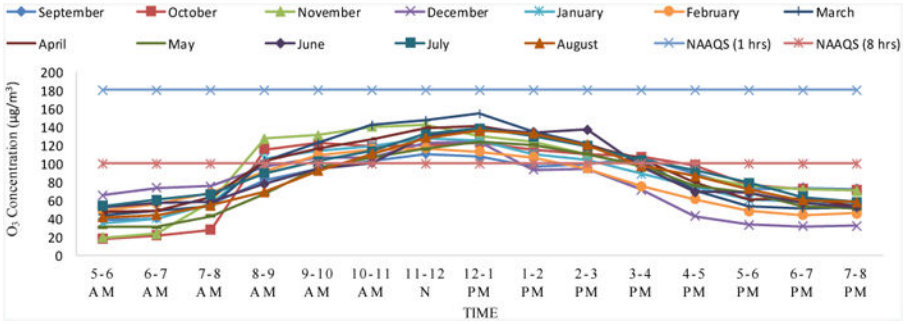

Fig. 2.
Diurnal variation of daily average ozone concentration.

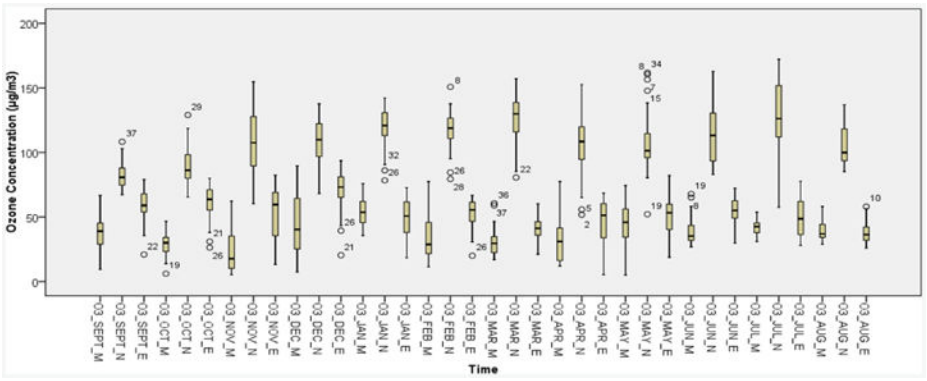

Fig. 3.

Spatial variations of ozone concentration for each month (September 2014–August 2015) during morning, day and evening time.

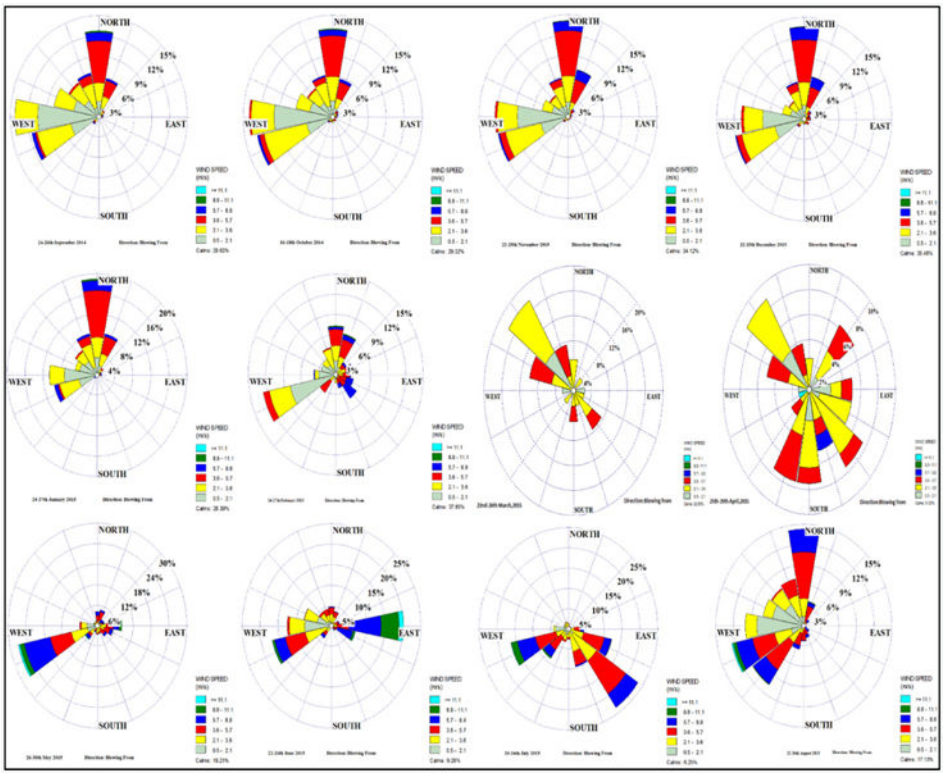

Fig. 4.

Wind-rose diagram for the hourly wind speed and wind direction data monitored during the sampling period in each month (September 2014–August 2015).

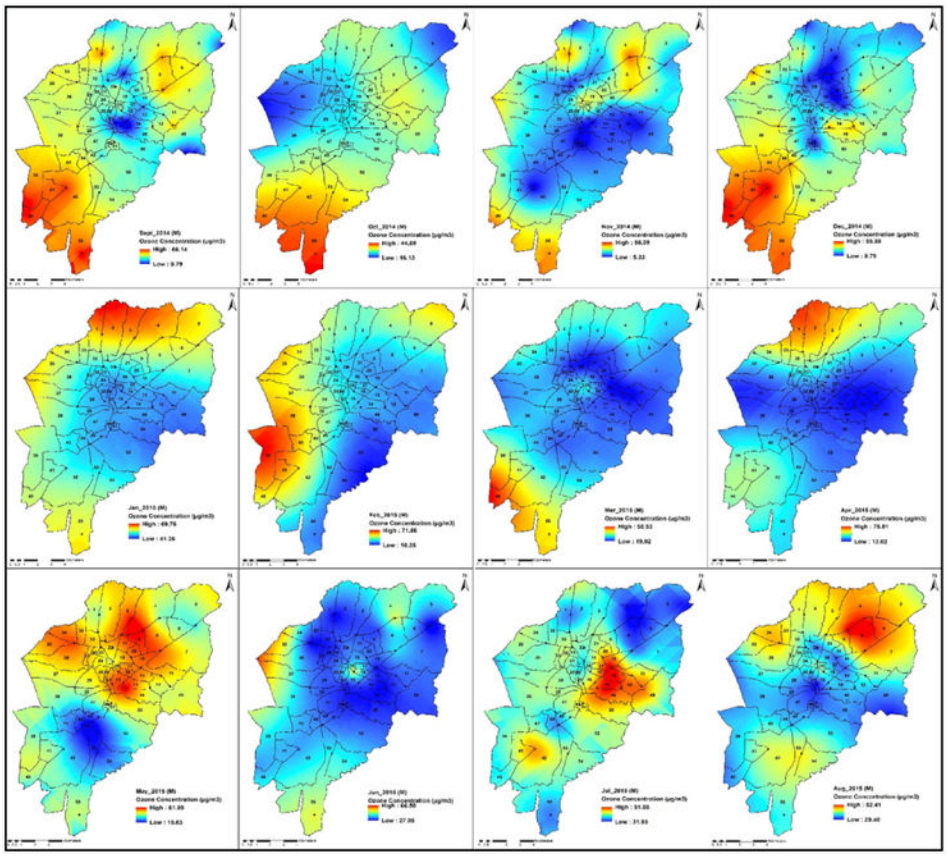

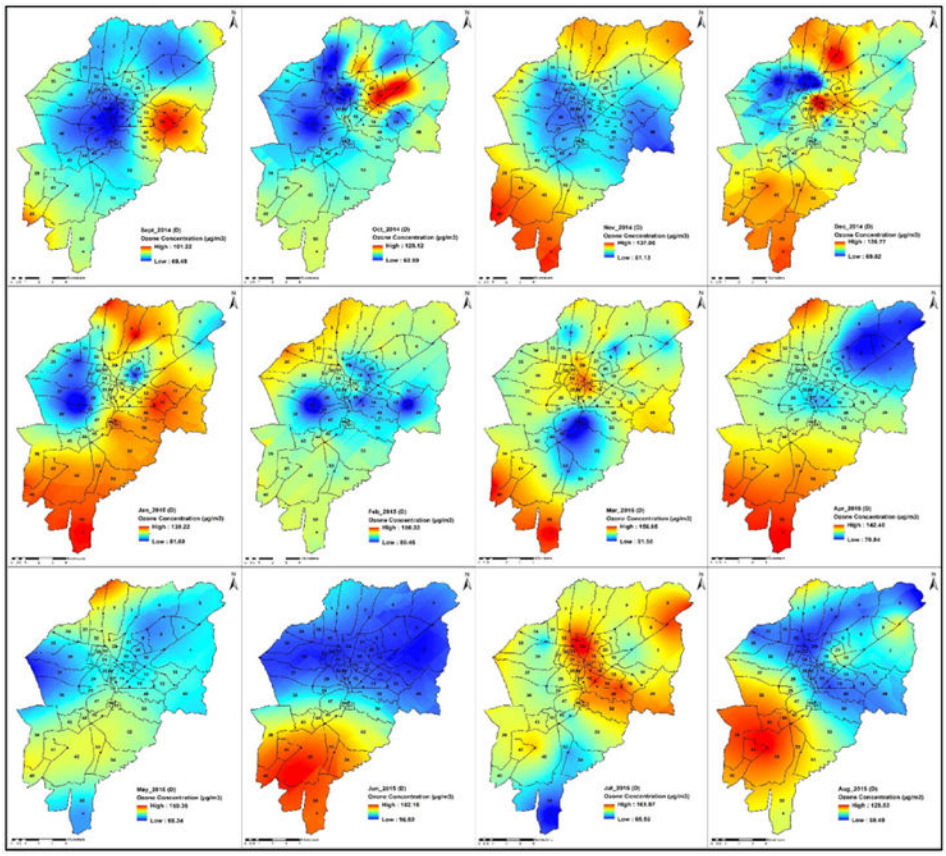

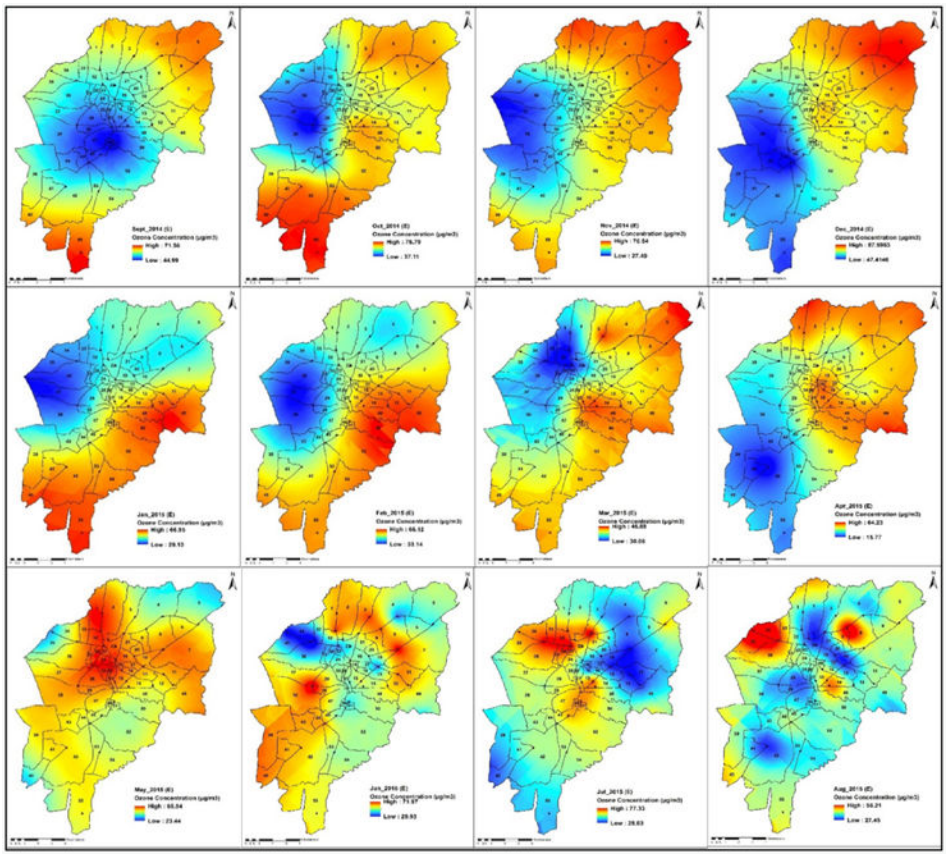

Fig. 5.

1. Spatial distributions of GLO concentration during morning-time for 12 months.

2. Spatial distributions of GLO concentration during day-time for 12 months.

3. Spatial distributions of GLO concentration during evening-time for 12 month.

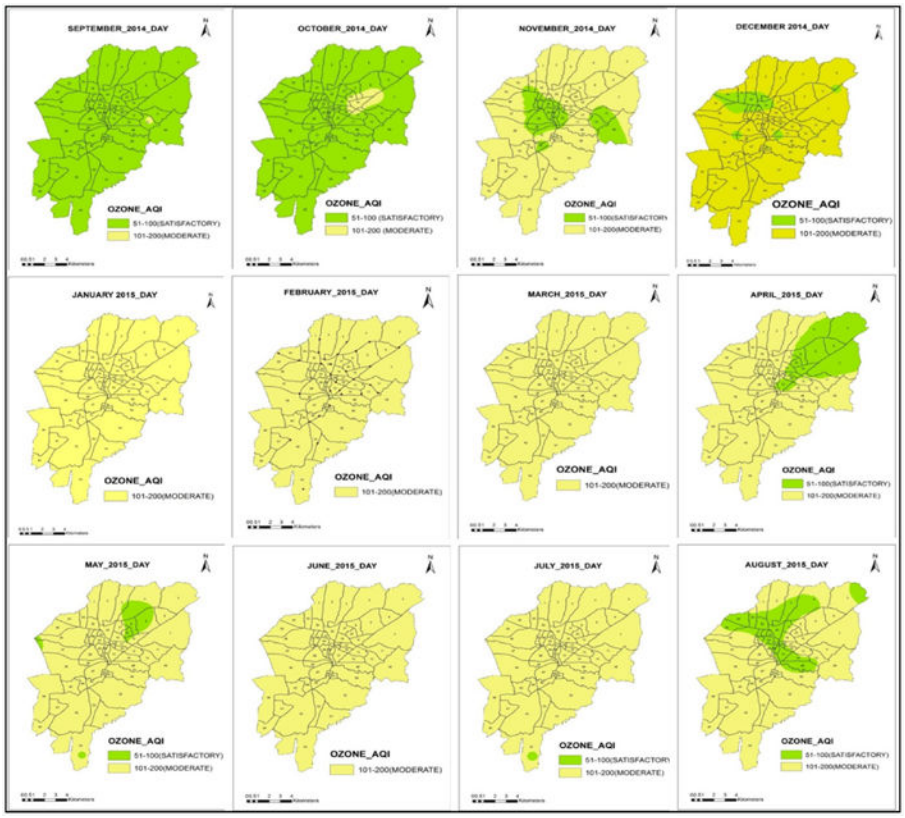

Fig. 6.
OZAQI maps in each month during daytime.

Table 1

Descriptive statistics of spatial distribution of ozone concentration.

Month	Morning time				Day time				Evening time			
	Min	Max	Mean	SD	Min	Max	Mean	SD	Min	Max	Mean	SD
SEPT	9.41	66.6	37.77	14.22	67.23	108.2	82.5	9.55	20.97	78.99	58.94	12.07
OCT	6.1	46.8	28.6	8.99	65.46	128.93	88.42	14.11	26.26	79.95	61.66	12.94
NOV	5.29	62.33	23.45	15.24	60.17	154.64	108.32	24.41	13.13	82.35	54.63	19.6
DEC	7.45	89.57	43.9	24.21	68.08	137.59	107.52	17.86	20.38	93.58	71.25	15
JAN	35.53	75.92	53.91	9.82	78.34	142.1	119.73	14.79	18.42	72.72	49.47	14.88
FEB	11.37	77.42	34.21	16.42	79.38	150.72	117.71	14.02	19.99	66.64	53.25	10.28
MAR	17	60.6	30.4	10.18	80.56	157.19	125.96	18.82	21.2	60.2	40.04	8.94
APR	12	77.5	33.62	19.04	51.74	152.49	107.6	24.4	5.4	68.4	46.63	15.17
MAY	5.1	74.28	43.41	15.93	52.14	161.73	106.96	21.77	18.8	82.11	50.04	14.71
JUN	26.8	67.8	38.68	10.03	83	162.8	114.8	24.3	29.8	72.3	54.82	9.92
JUL	31	53.7	41.72	5.66	57.6	172.1	126.66	29.59	28	77.6	49.3	14.82
AUG	28.8	58.1	39.07	6.67	85.2	136.8	105.13	13.9	26	58	38.16	8.59

Note: Total number of sample in each case was 40, Min-Minimum in μg m^{-3}, Max- Maximum in (μg m^{-3}), SD-Standard deviation in μg m^{-3}, Mean in μg m^{-3}.

Table 2

Characteristics of variogram models.

Months	Time	Fitted Variogram Model	Nugget (Co)	Partial Sill (C)	Lag size (in m)	Range (in m)	$[C_0/(C_0+C)]$%	ME	RMSE	ASE	MSE	RMSSE
September 2014	Morning	Stable	0	195.35	676.8	5414.4	0.0	0.11	12.63	12.39	0.02	1.00
	Day	Stable	28.7	69.3	570.4	4563.6	29.3	−0.26	6.53	8.15	−0.02	0.82
	Evening	Spherical	84.8	88.88	1498.5	11988.6	48.8	−0.55	11.17	11.16	−0.03	1.01
October 2014	Morning	Stable	34.8	49.2	1002.8	8022.4	41.4	0.07	8.03	7.20	0.01	1.08
	Day	Gaussian	0.28	284.0	303.0	2424.4	0.1	−1.11	12.98	14.97	−0.04	0.98
	Evening	Exponential	55.2	151.8	1590.9	12727	26.7	−0.11	11.68	11.41	0.00	1.02
November 2014	Morning	Stable	0	183.9	700.3	5602.7	0.0	−1.72	12.18	10.88	−0.10	1.05
	Day	Exponential	282.7	482.7	2258.7	18069.6	36.9	−0.90	21.14	22.08	−0.03	0.98
	Evening	Stable	252.9	172.3	960.8	7686.8	59.5	−0.44	17.88	18.34	−0.01	0.98
December 2014	Morning	Stable	0	570.6	969.0	7752.7	0.0	−0.17	20.87	20.11	0.00	1.02
	Day	Exponential	0	439.6	319.0	2552.0	0.0	−1.34	14.53	20.89	−0.04	0.72
	Evening	Spherical	92.6	187.9	1511.4	12091.5	33.0	−0.03	13.52	12.79	0.00	1.05
January 2015	Morning	Stable	50.7	69.5	1101.6	8813.2	42.2	−0.35	7.52	8.53	−0.03	0.91
	Day	Exponential	18.52	250.9	802.9	6423.8	6.9	−0.28	13.55	13.77	−0.01	1.00
	Evening	Stable	126.8	115.1	882.1	7057.0	52.4	−0.18	12.46	13.84	−0.01	0.92
February 2015	Morning	Stable	63.0	302.6	1273.9	10191.6	17.2	0.02	13.98	10.54	0.00	1.29
	Day	Stable	0	151.7	452.8	3623.1	0.0	−1.92	12.00	11.71	−0.13	1.01
	Evening	Gaussian	47.1	86.7	960.8	7686.7	35.2	−0.70	8.60	8.70	−0.06	0.95
March 2015	Morning	Spherical	12.2	81.7	1020.0	8160.7	13.0	−0.49	7.01	6.91	−0.04	1.01
	Day	Stable	0	380.9	867.1	6937.4	0.0	−0.90	16.41	16.15	−0.03	1.00
	Evening	Exponential	46.4	42.7	874.6	6997.0	52.1	−0.41	8.57	9.01	−0.03	0.95
April 2015	Morning	Stable	117.5	372.2	1064.6	8517.0	24.0	−0.44	11.26	14.36	−0.02	0.77
	Day	Spherical	140.3	646.5	1577.4	12619.5	17.8	−0.95	16.80	18.52	−0.03	0.97
	Evening	Exponential	72.4	209.0	1646.3	13170.5	25.7	−0.33	12.12	13.14	−0.01	0.94
May 2015	Morning	Spherical	70.0	201.5	580.2	4642.3	25.8	0.14	13.67	14.79	0.01	0.95
	Day	Spherical	115.5	435.4	1295.9	10367.3	21.0	0.15	19.81	16.78	0.00	1.07
	Evening	Gaussian	71.3	170.3	852.4	6819.8	29.5	0.58	12.84	11.43	0.05	1.12

Table 3

Breakpoint concentration of air pollutants defined in IND-AQI system (Sharma *et al.*, 2003).

Breakpoints O_3 **(μg** m^{-3}**) 8-hour**	**OZAQI**	**Category**	**Health Impacts**
50	0–50	Good	No health problems
100	51–100	Satisfactory	May cause breathing problem to sensitive people
168	101–200	Moderate	May cause asthma and other breathing problem to children and older adults
208	201–300	Poor	May cause breathing problem with heart disease to normal healthy people
748**	301–400	Very Poor	May cause lung and heart disease and respiratory illness to healthy people
748+**	> 400	Severe	May cause serious health problem even during light physical activity to the healthy people and increase the rate of mortality

** 1-hr monitoring values.